Catalysis Today 158 (2010) 263–268

Contents lists available at ScienceDirect

Catalysis Today

journal homepage: www.elsevier.com/locate/cattod

Electrochemical catalysis and stability of tetraamido macrocyclic ligands iron immobilized on modified pyrolytic graphite electrode

Jinghua Wang[a], Hong Sun[a,*], X.S. Zhao[a,b]

[a] Institute of Multifunctional Materials (IMM), Laboratory of New Fiber Materials and Modern Textile, College of Chemistry, Chemical Engineering and Environment, Qingdao University, Ningxia Road 308, Qingdao 266071, China
[b] Department of Chemical and Biomolecular Engineering, National University of Singapore, 4 Engineering Drive 4, Singapore 117576, Singapore

ARTICLE INFO

Article history:
Available online 18 April 2010

Keywords:
Tetraamido macrocyclic ligands iron
Sodium alginate
Electrochemistry
Electrocatalysis
Sensor

ABSTRACT

A synthetic molecule tetraamido macrocyclic ligands iron complex (Fe^{III}-TAML), a catalyst that speeds up peroxide oxidation reaction, was immobilized on pyrolytic graphite (PG) electrode modified with sodium alginate (SA) gel films. The tetraamido macrocyclic ligands iron complex in the sodium alginate thin films was characterized by cyclic voltammetry (CV), ultraviolet–visible spectrophotometry (UV–vis) and scanning electron microscopy (SEM). The characterization results showed that the tetraamido macrocyclic ligands iron complex on pyrolytic graphite electrode retained its native structure and displayed a pair of well-defined and nearly reversible peaks at about −0.051 V and 0.051 V (V vs saturated calomel electrode, SCE) in a 0.1 M phosphate buffer solution of pH 7.0, originated from the tetraamido macrocyclic ligands iron complex redox couples. The iron complex in the sodium alginate films also exhibited a good electrocatalytic property toward the decomposition of hydrogen peroxide with a significant lowering of overpotential, indicating the electrode can be potential hydrogen peroxide sensors. The amperometric response of the sensor which showed good stability and reliability varied linearly with the hydrogen peroxide concentrations ranging from 2.2 mM to 24 mM, with a detection limit of 0.88 mM at a signal-to-noise ratio of 3.

1. Introduction

The determination of hydrogen peroxide (H_2O_2) has become extremely important in recent years because H_2O_2 is widely used in the food, medicine, chemical and biochemical industries, as well as for environmental analysis [1–4]. Many techniques have been employed for H_2O_2 detection such as titrimetry [5], spectrometry [6], chemiluminescence [7] and electrochemistry [8–11]. The electrochemistry methods based on a simple and low-cost enzyme electrode have attracted much attention [12–14]. However, one common drawback of the enzyme-based H_2O_2 sensors is the poor stability originated from the nature of the enzymes. Because the enzymes are easy to deform thermally and chemically during fabrication, storage or application, their catalytic activities can be easily lost, which limit their technological applicability [15,16]. This problem has driven chemists to design and fabricate low-molecule, enzyme-free electrocatalysts [17–21], which are electrocatalytically active, yet stable against aggressively oxidizing acidic and basic environments [22].

The biomimetic oxidation chemistry of synthetic iron porphyrins [23,24] and non-heme iron complexes [25–30] has also been widely investigated. Over the last two decades, a large amount of oxidatively robust iron complexes were developed and used as sensors for electrochemical determination of hydrogen peroxide, organic hydroperoxides captopril [31,32], fenitrothion [33], toxic metal cations [34,35], and even the explosive [36,37].

Tetraamido macrocyclic ligands iron complex, an oxidant activator, was first developed by Collins [38,39]. Fe^{III}-TAML molecule features an iron atom in its center, surrounded by four nitrogen atoms, which in turn is corralled by a ring of carbon atoms (Scheme 1). X-ray diffraction structure analysis demonstrated the presence of 5-coordination (5-CN) with Fe–OH_2 bonds [40,41]. The mechanism of the oxidant activation of TAML to peroxide is that when hydrogen peroxide is present, it can displace a water ligand and create a catalyst that triggers oxidation reactions with other compounds in the solution.

The Fe(III) center of the nontoxic catalyst can coordinate to tetraamido macrocyclic ligands, giving a Fe^{III}-TAML oxidant activator, which catalyzes a variety of technologically important oxidation reactions by hydrogen peroxide in water [39,42]. These include the rapid leaching of water soluble dyes [43], the decolorization of pulp mill effluents, the delignification of wood pulp [44], the complete remediation of chlorophenol persistent pollu-

* Corresponding author. Tel.: +86 532 83780323; fax: +86 532 85955529.
E-mail addresses: sun_hong@qdu.edu.cn, qdusunhong@hotmail.com (H. Sun).

0920-5861/$ – see front matter © 2010 Elsevier B.V. All rights reserved.
doi:10.1016/j.cattod.2010.03.046

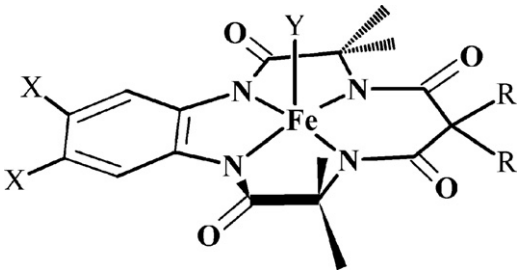

Scheme 1. The structure of TAML activator. X = Cl, Y = H_2O, R = CH_3.

tants [45], and the selective oxidation of thiophene compounds of gasoline and diesel [46–48]. Fe^{III}-TAML has the similar catalytic mechanism with some enzymes, such as horseradish peroxidase (HRP) and cytochrome P450. It can combine with peroxide molecules and speed up the release rate of free radicals [49,50]. Fe^{III}-TAML activators are exceptionally active; the second order rate constant for the rate-limiting activation of H_2O_2 was determined to be as high as 10^4 M^{-1} s^{-1} at 25 °C and an optimal pH [51]. TAML catalysts are effective in nanomolar to low micromolar concentrations in water where they can attain turnover frequencies in thousands per minute. It is a novel class of oxidatively robust "green" catalyst [52,53], which provides the first highly effective small molecule mimics of peroxidase enzymes, yet the TAML system was discovered to be innocent [47,54].

Alginate, an anionic polysaccharide, has been widely used as an instant gel for bone tissue engineering owing to its good biocompatibility [55–57]. Recently, Zhao et al. [58] employed sodium alginate (SA) as a matrix to immobilize hemoglobin on multiwalled carbon nanotubes for electrochemical biosensor applications.

In this paper, we described an approach to immobilizing Fe^{III}-TAML in SA films on pyrolytic graphite (PG) electrodes. Various techniques were used to characterize the Fe^{III}-TAML/SA films. The electrochemical properties of the Fe^{III}-TAML were characterized by using cyclic voltammetry (CV). The Fe^{III}-TAML immobilized in SA films exhibited well-defined and reversible electrochemistry features with reversible redox properties and a pair of redox peaks at about −0.051 and 0.051 (V vs SCE). Moreover, in accordance with its activity in the solution, the immobilized Fe ligand displayed a very good electrocatalytic performance toward hydrogen peroxide. A new peroxide sensor was then fabricated by utilizing this immobilized Fe^{III}-TAML as mimetic enzyme electrode. Compared with enzyme-based H_2O_2 sensors, the Fe^{III}-TAML-based peroxide sensor displayed unique properties, such as a better thermal stability.

2. Experimental

2.1. Chemicals and reagents

The Fe^{III}-TAML was synthesized according to Collins et al. [59] and He et al. [60] and characterized with Fourier transform infrared spectroscopy (FT-IR), Ultraviolet–visible spectrophotometry (UV–vis) and elements analysis. Sodium Alginate was from Qingdao Huadong Chemicals. Hydrogen peroxide (H_2O_2, 30%) was from Qingdao Chemical Engineering Plant. All other chemicals were of analytical grade.

The electrolyte was usually 0.05 M potassium dihydrogen phosphate buffers at pH 7.0 containing 0.1 M KBr. Other buffers were 0.1 M sodium acetate, 0.1 M boric acid, and 0.1 M citric acid, all containing 0.1 M KBr. The pHs of buffers were regulated with a HCl or NaOH solution.

2.2. Preparation of Fe^{III}-TAML/SA composite modified electrodes

Prior to use, the PG electrode (PG, 3 mm diameter) was polished first with metallographic sandpapers while flushing with water and then polished on a clean billiard cloth with twice distilled water. The electrodes were ultrasonicated in distilled water for 30 s after each polishing step. Then it was dried under nitrogen.

The amount of Fe^{III}-TAML was controlled by a micro-syringe. We have studied the relationship between the peak current of a CV curve and the amount of Fe^{III}-TAML used (2, 4, 6, 8, 10, 12, 14, and 16 μL of 1 mg/mL Fe^{III}-TAML solutions were used in this study). The peak current reached the highest with 10 μL of 1 mg/mL Fe^{III}-TAML solution. So, the electrode modified with 10 μL of 1 mg/mL Fe^{III}-TAML solution was chosen to detect hydrogen peroxide.

The experimental conditions for preparation of Fe^{III}-TAML/SA composite modified electrodes were optimized after a series of experiments.

Typically, 5 μL of 1 mg/mL SA solution was spread evenly onto a freshly polished PG electrode with a micro-syringe. A small bottle was fit tightly over the electrode to serve as a closed evaporation chamber for several hours so that the water was evaporated slowly and more uniform films were formed. After the films stood overnight, 10 μL of 1 mg/mL Fe^{III}-TAML solution was spread onto the dry SA film surface with a micro-syringe. A small bottle was fit tightly over the electrode so that water evaporated gradually. The Fe^{III}-TAML/SA films were then dried in air overnight.

To investigate the formation of Fe^{III}-TAML/SA films, a glass slide was substituted PG electrode and the formation process of Fe^{III}-TAML/SA film on glass surface was performed by the same process. After dried in air overnight, the glass slide was tested by Thermal Fished EV-300 UV spectrophotometer.

2.3. Instruments and procedures

A CHI 760C electrochemical analyzer (CH Instruments) was used for CV. In electrochemical measurements, a regular three-electrode cell was used with a saturated calomel electrode (SCE) as reference, a platinum wire as counter electrode, and a PG electrode coated with films as working electrode. All experiments were performed at ambient temperature (20 ± 2 °C).

Voltammetry on Fe^{III}-TAML/SA film electrodes was carried on in buffers. Prior to electrochemical measurements, buffer solutions were purged with purified nitrogen for at least 15 min, and then the nitrogen was bubbled gently through the solutions for exclusion of oxygen during the whole experiments. In the experiments, measured volumes of hydrogen peroxide were injected via a syringe to solutions in a sealed cell, which had been previously degassed with nitrogen.

UV–vis absorption spectroscopy was measured with a Thermal Fished EV-300 UV spectrophotometer. SEM was done with a JSM-6390LV scanning electron microanalyzer at an acceleration voltage of 20 kV. FT-IR spectra were measured with Nicolet 5700 spectrophotometer. Elemental analyses were performed on a vario EL III Elementar (Germany). Sample films for SEM, UV–vis and FT-IR were prepared on the glass slides.

3. Results and discussion

3.1. Synthesis of complexes

The Fe^{III}-TAML was prepared according to described procedures. The solid was recrystallized from acetonitrile–water (1:1, v/v), the resulting orange crystalline material was dried in a vacuum over 5 h at 45 °C. 30% Activators were synthesized in aqua forms. The Fe^{III}-TAML was identified by IR, UV, and elemental analysis.

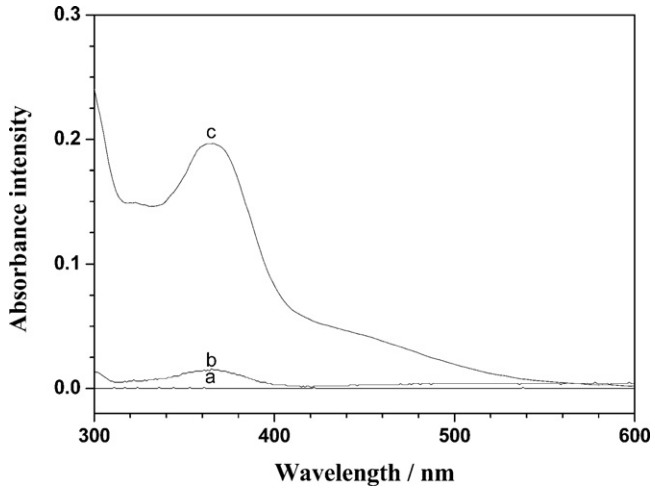

Fig. 1. UV–vis spectra for (a) SA precursor film, (b) Fe^{III}-TAML/SA films on glass slide surface and (c) Fe^{III}-TAML in aqueous solution.

Anal. calcd for $C_{19}H_{20}N_4FeO_4Cl_2.(H_2O)$: C, 44.444; H, 4.288; N, 10.916, and C/N, 4.071; experiment for: C, 42.19; H, 5.139; N, 9.272; and C/N, 4.550.

IR (KBr) ν [cm^{-1}]: 3417, 1699, 1629 (CON–), 1118 (C–N), 1375($-CH_3$).

3.2. Conformational studies

UV–vis spectroscopy was used to characterize the structure of Fe^{III}-TAML in solution and within SA films. A typical absorption spectrum of Fe^{III}-TAML in deionized (DI) water solution was depicted in Fig. 1c.

To investigate the immobilization process of Fe^{III}-TAML in SA film surface, a clean glass slide was used to test the UV phenomenon. The immobilization process was performed by using the same procedures, typically, the SA film was coated onto fresh clean glass surface first and then one drop of Fe^{III}-TAML solution was dropped onto SA film surface. After Fe^{III}-TAML treatment, films were blown dry in air and kept at room temperature overnight to dry. Then films were immersed into DI water for about 1 h, non-absorbed Fe^{III}-TAML on the film surface would be washed and the slides could be used for the UV spectrum test. A typical absorption spectrum of Fe^{III}-TAML/SA film was depicted in Fig. 1b. Compared with glass slide with SA film only (Fig. 1a), an absorption peak of TAML was obtained at about 368 nm (Fig. 1b), which was in accordance with the data obtained from aqueous solution. Both Fe^{III}-TAML in solution (Fig. 1c) and Fe^{III}-TAML/SA films demonstrated absorption band at 368 nm, indicating that Fe^{III}-TAML in dry films retained its native structure.

The adsorption bands of CON– for native Fe^{III}-TAML were observed at 3417 cm^{-1}, 1629 cm^{-1}, 1118 cm^{-1}(C–N), respectively. Similar characteristic peaks (3419 cm^{-1} and 1627 cm^{-1} for CON–, 1134 cm^{-1} for C–N) were observed for the Fe^{III}-TAML immobilized on the SA composite film at this time. The similarity of the Fe^{III}-TAML and Fe^{III}-TAML/SA spectra revealed that the Fe^{III}-TAML immobilized on the SA composite film almost retained its original structure.

3.3. Morphology of Fe^{III}-TAML/SA films

Scanning electron microscopy (SEM) was then used to characterize the morphology of SA and Fe^{III}-TAML/SA films on glass slides. SA film presented a smooth surface (Fig. 2a) and a much different morphology of Fe^{III}-TAML/SA films as shown in Fig. 2b was observed compared to the SA film only. In addition, the SEM

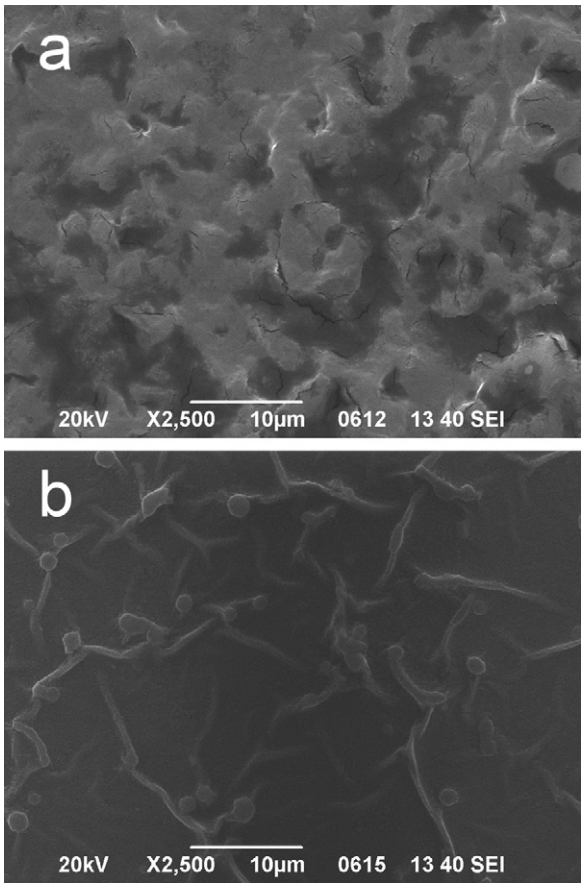

Fig. 2. Top view of SEM for (a) SA, and (b) Fe^{III}-TAML/SA films with the same magnification.

cross-sectional views technique was used to estimate the thickness of Fe^{III}-TAML/SA films after freeze-fracturing, which was about 3–5 μm.

3.4. Electrochemical properties of Fe^{III}-TAML

Electrochemical characteristics derived from CV reflected the nature of Fe^{III}-TAML. When a Fe^{III}-TAML/SA films electrode was immersed into pH 7.0 buffer solutions containing no Fe^{III}-TAML, after about 15 min of soak and several CV scan, a pair of peaks at the steady state were observed at about −0.051 V and 0.051 V (V vs SCE). Fig. 3b shows a single electrochemically reversible redox process at electrode, in accordance with characteristic of the Fe(III)/Fe(II) redox couples [61]. The peaks of Fe^{III}-TAML/SA films showed nearly reversible cyclic voltammograms in blank buffers, suggesting direct electron transfer occurred between Fe^{III}-TAML and PG electrode in SA films.

Fe^{III}-TAML/SA films in pH 7.0 buffers showed quite symmetrical peak shape (Fig. 3) with roughly equal heights of reduction and oxidation peaks. Fig. 4 shows that the reduction peak currents increased linearly with scan rates from 0.1 V s^{-1} to 0.8 V s^{-1}, and integration of reduction peaks at different scan rates in this range gave nearly constant charge (Q) values. Moreover, the anodic peak current increased linearly with the scan rates, as shown in the insert of Fig. 4. All these are characteristic of diffusionless, surface-confined voltammetric behavior [62].

3.5. Catalytic activity

Catalytic CV behavior was also observed for hydrogen peroxide at Fe^{III}-TAML/SA film electrodes. Take Fe^{III}-TAML/SA film electrode

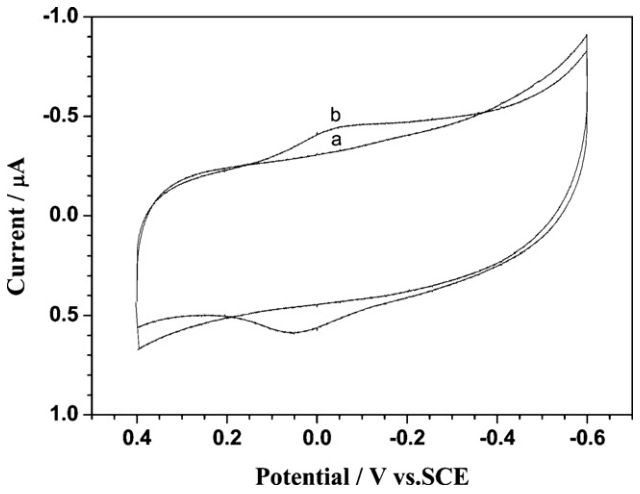

Fig. 3. Cyclic voltammograms for (a). SA films; (b). Fe^{III}-TAML/SA films at 0.2 V s^{-1} in pH 7.0 buffers.

as an example, when H_2O_2 was added to a pH 7.0 buffer, an increase in reduction peak at about −0.4 V was observed with the disappearance of oxidation peak for Fe^{III}-TAML. The reduction peak current increased with the concentration of H_2O_2 in solution. However, the direct reduction of H_2O_2 was observed on SA precursor films at about −0.8 V (as shown in Fig. 5).

The electrocatalytic reduction of H_2O_2 at Fe^{III}-TAML/SA films was also tested by amperometry. Fig. 6 illustrated a typical amperometric response of Fe^{III}-TAML/SA films with the stepwise addition of H_2O_2 at the constant potential of −0.1 V vs SCE. The stepped increase of H_2O_2 concentration in buffers caused the corresponding growth of catalytic reduction currents with a linear relationship. While SA films without Fe^{III}-TAML also displayed some catalytic activity toward H_2O_2 reduction in amperometry, Fe^{III}-TAML/SA films behaved much better.

The left top of Fig. 6 shows the corresponding calibration curve of the sensor for H_2O_2 addition. The response to H_2O_2 was linear in the concentration range from 2.2 mM to 24 mM (R^2 = 0.998). The detection limit was 0.88 mM at a signal-to-noise ration of 3. The calibration curve tended to lever off when the concentration of H_2O_2 became larger. Association constants are evaluated and presented in Table 1.

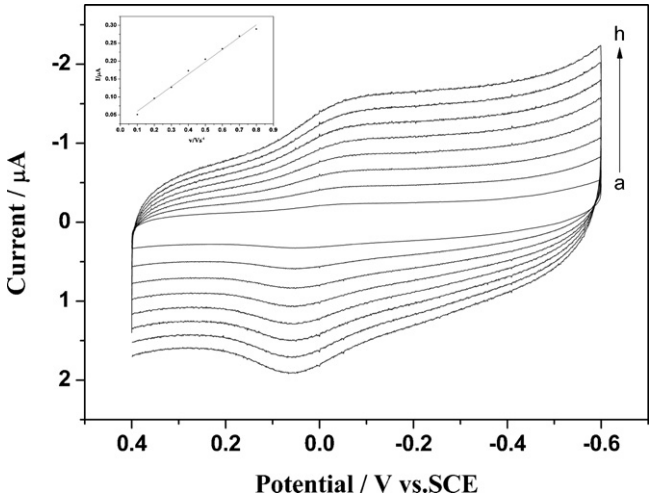

Fig. 4. Cyclic voltammograms of Fe^{III}-TAML/SA films in pH 5.5 buffers at scan rates of (from inner to outer): (a) 0.1, (b) 0.2, (c) 0.3, (d) 0.4, (e) 0.5, (f) 0.6, (g) 0.7, (h) 0.8 V s^{-1}. Inset shows the relationship between the anodic peak currents and scan rates.

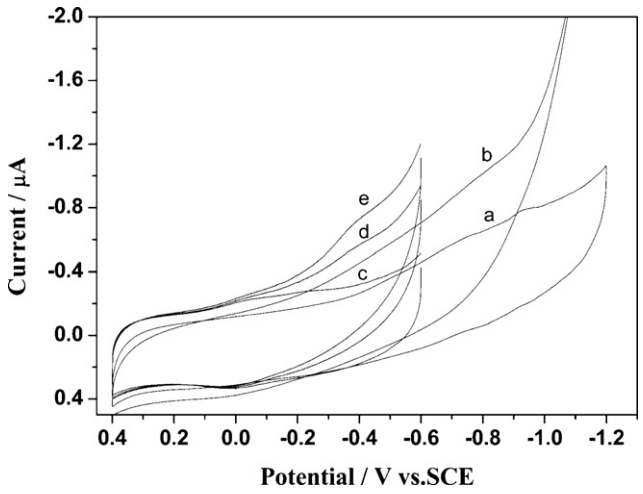

Fig. 5. Cyclic voltammograms at 0.1 V s^{-1} in pH 7.0 buffers for (a) SA film without H_2O_2, (b) SA film with 4.4 mM H_2O_2, (c) Fe^{III}-TAML/SA films without H_2O_2, (d) Fe^{III}-TAML/SA films with 2.2 mM H_2O_2, and (e) Fe^{III}-TAML/SA films with 4.4 mM H_2O_2.

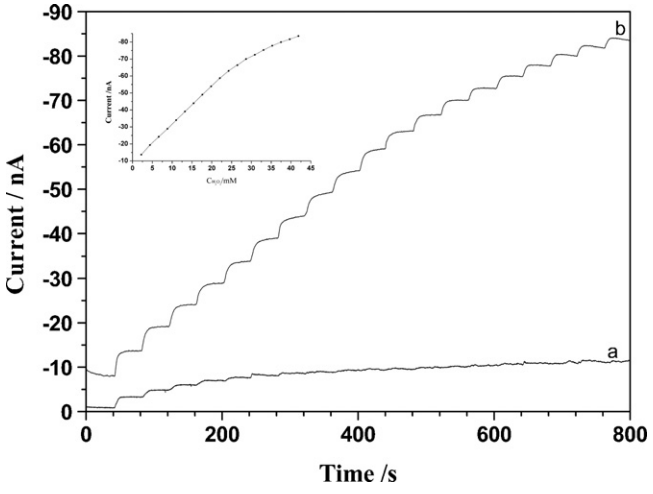

Fig. 6. Amperometric response of (a) SA film and (b) Fe^{III}-TAML/SA films at −0.1 V in pH 7.0 buffers solution with 2.2 mM H_2O_2 injected every 40s. Inset shows the calibration curves for H_2O_2 in pH 7.0 buffers for Fe^{III}-TAML/SA films.

The presence of the discrepancy of linear range and detection limit was understandable because different detection methods possessed different sensitivity. But the calculated characteristic constant had no obvious discrepancy, it was accordance with the theoretical phenomena because all of the detection conditions were just the same.

3.6. Stability of the sensor

The stability of Fe^{III}-TAML/SA films was tested by CV with two different storage methods. The first one was performed with wet storage method. PG electrodes coated with Fe^{III}-TAML/SA films were stored in pH 7.0 blank buffers and CVs were carried out period-

Table 1
Catalytic performances of Fe^{III}-TAML/SA films toward H_2O_2.

H_2O_2	Fe^{III}-TAML/SA film
Linear range (mM)	2.2–24
Detection limit (mM)	0.88
Sensitivity (nA mM^{-1})	2.24
Correlation coefficient	0.9996
Catalysis efficiency	4.879

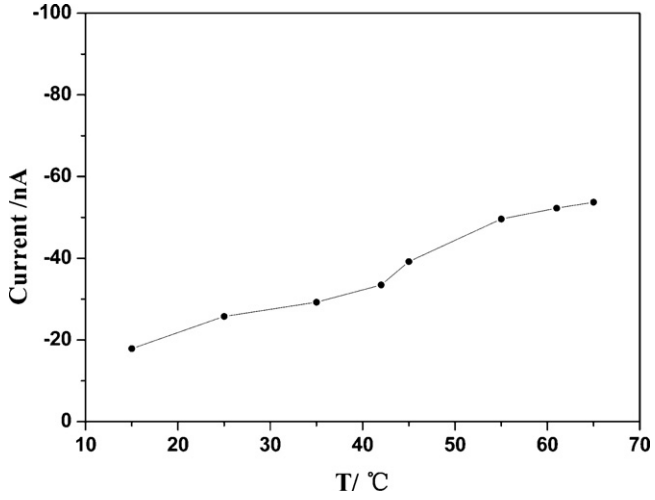

Fig. 7. Temperature effect on the amperometric response to 2.2 mM H_2O_2 in pH 7.0 buffers.

ically. The second method was dry storage method, Fe^{III}-TAML/SA film electrodes were stored in air for most of the storage time, and the test was performed in pH 7.0 buffers occasionally. The excellent stabilities of Fe^{III}-TAML/SA films were obtained from two methods. Peak potentials and currents of Fe^{III}-TAML/SA films electrode stored in wet and dry state essentially maintained unchanged for at least 1 month.

The enhanced thermo-stability of the sensor was tested. The current of the sensor to H_2O_2 in buffers increased slightly from 15 °C to 65 °C. Furthermore, the sensor still maintained a similar response without obvious deactivation at high temperatures (Fig. 7).

The operational stability of the sensor was examined with intermittent measuring the current response to 2.2 mM H_2O_2 in the stirred buffers every 12 h in the period of 3 days. The results illustrated the remaining activities of TAML related to the initial TAML activity. The storage stability of the sensor to 2.2 mM H_2O_2 in buffers was studied over the period of 2 months. The sensor was stored in buffers in the refrigerator at 4 °C when not in use. The catalytic current response could maintain about 70% of the initial signal, which demonstrated that the sensor operated in buffers in room temperature displayed good operational and storage stabilization.

4. Conclusions

Water soluble Fe^{III}-TAML was first incorporated into negatively charged sodium alginate (SA) gel film on pyrolytic graphite (PG) electrodes, forming Fe^{III}-TAML/SA films. The special structure of SA can form stable films on PG electrodes, which could hold the Fe^{III}-TAML immobilized stably and prevent it bleaching from the film. These ordered films are presumably stabilized mainly by electrostatic attractions between SA and Fe^{III}-TAML.

The modified electrode exhibited well-defined and nearly reversible electrochemistry features. The stable films showed catalytic properties to hydrogen peroxide with a significant lowering of overpotential. A new peroxide sensor was fabricated with this film which showed a linear range between 2.2 mM to 24 mM. Experimental data showed that such immobilized Fe^{III}-TAML system can be potential electrochemical sensors.

Acknowledgements

We thank the financial support of the Qingdao University Science Foundation and the Growing Base for State key Laboratry of Qingdao University is gratefully acknowledged. The Taishan Scholars Program of Shangdong Province is acknowledged.

References

[1] J. Wang, Y. Lin, L. Chen, Organic-phase biosensors for monitoring phenol and hydrogen peroxide in pharmaceutical antibacterial products, Analyst 118 (1993) 277–280.
[2] E.S. Forzani, G.A. Rivas, V.M. Solis, Amperometric determination of dopamine on an enzymatically modified carbon paste electrode, J. Electroanal. Chem. 382 (1995) 33–40.
[3] T. Ruzgas, E. Csöegi, J. Emneus, L. Gorton, G. Marko-Varga, Peroxidase-modified electrodes: fundamentals and application, Anal. Chim. Acta 330 (1996) 123–138.
[4] L. Wang, E. Wang, A novel hydrogen peroxide sensor based on horseradish peroxidase immobilized on colloidal Au modified ITO electrode, Electrochem. Commun. 6 (2004) 225–229.
[5] E.C. Hurdis, J.H. Romeyn, Accuracy of determination of hydrogen peroxide by cerateoxidimetry, Anal. Chem. 26 (1954) 320–325.
[6] R. Santucci, E. Laurenti, F. Sinibaldi, R.P. Ferrari, Effect of dimethyl sulfoxide on the structure and the functional properties of horseradish peroxidase as observed by spectroscopy and cyclic voltammetry, Biochim. Biophys. Acta 1596 (2002) 225–233.
[7] L. Luo, Z. Zhang, Sensors based on galvanic cell generated electrochemiluminescence and its application, Anal. Chim. Acta 580 (2006) 14–17.
[8] Y. Miao, S.N. Tan, Amperometric hydrogen peroxide biosensor based on immobilization of peroxidase in chitosan matrix crosslinked with glutaraldehyde, Analyst 125 (2000) 1591–1594.
[9] S.Q. Liu, H.X. Ju, Renewable reagentless hydrogen peroxide sensor based on direct electron transfer of horseradish peroxidase immobilized on colloidal gold-modified electrode, Anal. Biochem. 307 (2002) 110–116.
[10] K.S. Tseng, L.C. Chen, K.C. Ho, Amperometric detection of hydrogen peroxide at prussian blue-modified FTO electrode, Sens. Actuator B: Chem. 108 (2005) 738–745.
[11] Y. Lin, X. Cui, L. Li, Low-potential amperometric determination of hydrogen peroxide with a carbon paste electrode modified with nanostructured cryptomelane-type manganese oxides, Electrochem. Commun. 7 (2005) 166–172.
[12] C. Guo, Y. Song, H. Wei, P. Li, L. Wang, L. Sun, Y. Sun, Z. Li, Room temperature ionic liquid doped DNA network immobilized horseradish peroxidase biosensor for amperometric determination of hydrogen peroxide, Anal. Bioanal. Chem. 389 (2007) 527–532.
[13] Y.H. Song, L. Wang, C.B. Ren, G.Y. Zhu, Z. Li, A novel hydrogen peroxide sensor based on horseradish peroxidase immobilized in DNA films on a gold electrode, Sens. Actuators B: Chem. 114 (2006) 1001–1006.
[14] E. Ferapontova, K. Schmengler, T. Borchers, T. Ruzgas, L. Gorton, Effect of cysteine mutations on direct electron transfer of horseradish peroxidase on gold, Biosens. Bioelectron. 17 (2002) 953–963.
[15] A. Fersht, Structure and Mechanism in Protein Science: A Guide to Enzyme Catalysis and Protein Folding, W.H. Freeman, New York, 1999.
[16] H.B. Dunford, Heme Peroxidases, Wiley–VCH, New York, 1999.
[17] A. Sorokin, J.L. Seris, B. Meunier, Efficient oxidative dechlorination and aromatic ring cleavage of chlorinated phenols catalyzed by iron sulfophthalocyanine, Science 268 (1995) 1163–1166.
[18] M.C. White, A.G. Doyle, E.N. Jacobsen, A synthetically useful, self-assembling MMO mimic system for catalytic alkene epoxidation with aqueous H_2O_2, J. Am. Chem. Soc. 123 (2001) 7194–7195.
[19] Z.W. Xi, N. Zhou, Y. Sun, K.L. Li, Reaction-controlled phase-transfer catalysis for propylene epoxidation to propylene oxide, Science 292 (2001) 1139–1141.
[20] K. Kamata, K. Yonehara, Y. Sumida, K. Yamaguchi, S. Hikichi, N. Mizuno, Efficient epoxidation of olefins with ≥99% selectivity and use of hydrogen peroxide, Science 300 (2003) 964–966.
[21] M.-J. Song, S.W. Hwang, D. Whang, Non-enzymatic electrochemical CuO nano flowers sensor for hydrogen peroxide detection, Talanta 80 (2010) 1648–1652.
[22] A. Ghosh, A.D. Ryabov, S.M. Mayer, D.C. Horner, D.E. Prasuhn Jr., G.S. Sen, L. Vuocolo, C. Culver, M.P. Hendrich, C.E. Rickard, R.E. Norman, C.P. Horwitz, T.J. Collins, Understanding the mechanism of H(+)-induced demetalation as a design strategy for robust iron(III) peroxide-activating catalysts, J. Am. Chem. Soc. 125 (2003) 12378–12379.
[23] Y. Watanabe, Model studies on heme monooxygenases, in: T. Funabiki (Ed.), Oxygenases and Model Systems, Kluwer Academic Publishers, Dordrecht/Boston/London, 1996, pp. 223–282.
[24] Y. Watanbe, H. Fujii, Characterization of high-valent oxo-metalloporphyrins, Struct. Bond. 97 (2000) 61–89.
[25] M. Costas, M.P. Mehn, M.P. Jensen, L. Que Jr., Oxygen activation at mononuclear nonheme iron: enzymes, intermediates, and models, Chem. Rev. 104 (2004) 939–986.
[26] T. Funabiki, Introduction—developments in enzymatic and model studies on oxygenases, in: T. Funabiki (Ed.), Oxygenases and Model Systems, Kluwer Academic Publishers, Dordrecht/Boston/London, 1996, pp. 1–393.
[27] T. Funabiki, Catalysis by metal complexes, in: L.I. Simandi (Ed.), Advances in Catalytic Activation of Dioxygen by Metal Complexes, Kluwer Academic Publishers, Dordrecht/Boston/London, 2003, pp. 157–226.

[28] J.-U. Rohde, M.R. Bukowski, L. Que Jr., Functional models for mononuclear nonheme iron enzymes, Curr. Opin. Chem. Biol. 7 (2003) 674–682.
[29] L.I. Simandi, T.M. Sinandi, Z. May, G. Besenyei, Catalytic activation of dioxygen by oximatocobalt(II) and oximatoiron(II) complexes for catecholase-mimetic oxidations of o-substituted phenols, Coord. Chem. Rev. 245 (2003) 85–93.
[30] C.E. MacBeth, A.P. Golombek, V.G. Young Jr., C. Yang, K. Kuczera, M.P. Hendrich, A.S. Borovik, O_2 activation by nonheme iron complexes: a monomeric Fe(III)-oxo complex derived from O_2, Science 289 (2000) 938–941.
[31] B. Rezaei, S. Damiri, Voltammetric behavior of multi-walled carbon nanotubes modified electrode-hexacyanoferrate(II) electrocatalyst system as a sensor for determination of captopril, Sens. Actuators B: Chem. 134 (2008) 324–331.
[32] J.C. Ndamanisha, L.P. Guo, G. Wang, Mesoporous carbon functionalized with ferrocenecarboxylic acid and its electrocatalytic properties, Microporous Mesoporous Mater. 113 (2008) 114–121.
[33] A. Chanda, S.K. Khetan, D. Banerjee, A. Ghosh, T.J. Collins, Tatal degration of fenitrothion and other organophosphorous pesticides by catalytic oxidation employing Fe-TAML peroxide activators, J. Am. Chem. Soc. 128 (2006) 12058–12059.
[34] W. Liu, M.L. Zhang, X. Li, M.P. Song, One-pot synthesis of 1,1′-ferrocenediylbis-(methyltriphenylphosphonium iodide) from the corresponding alcohols: facile precursor for the construction of novel metal cations electrochemical sensors, Inorg. Chem. Commun. 11 (2008) 694–698.
[35] K. Kowalski, R.F. Winter, The synthesis, structures, and electrochemistry of 1′-heteroaryl-2,5-dimethylazaferrocenes, J. Organomet. Chem. 693 (2008) 2181–2187.
[36] D.F. Laine, I.F. Cheng, Analysis of hydrogen peroxide and an organic hydroperoxide via the electrocatalytic fenton reaction, Microchem. J. 91 (2009) 78–81.
[37] D.F. Laine, I.F. Cheng, Electrochemical detection of the explosive, hexamethylene triperoxide diamine (HMTD), Microchem. J. 91 (2009) 125–128.
[38] T.J. Collin, R.D. Powell, C. Slebodnick, et al., Stable highly oxidizing cobalt complexes of macrocyclic ligands, J. Am. Chem. Soc. 113 (1991) 8419–8425.
[39] T.J. Collins, Designing ligands for oxidizing complexes, Acc. Chem. Res. 27 (1994) 279–285.
[40] M.J. Bartos, C. Kidwell, K.E. Kaufffmann, S.W. Gordon-Wylie, T.J. Collins, G.C. Clark, E. Münck, S.T. Weintraub, A stable aquairon(III) complex with S = 1: structure and spectroscopic properties, Angew. Chem. Int. Ed. Engl. 34 (1995) 1216–1219.
[41] M.J. Bartos, S.W. Gordon-Wylie, B.G. Fox, L.J. Wright, S.T. Weintraub, K.E. Kauffmann, E. Münck, K.L. Kostka, E.S. Uffelman, C.E.F. Rickard, K.R. Noon, T.J. Collins, Designing ligands to achieve robust oxidation catalysts. iron based systems, Coord. Chem. Rev. 174 (1998) 361–390.
[42] T.J. Collins, TAML oxidant activators: a new approach to the activation of hydrogen peroxide for environmentally significant problems, Acc. Chem. Res. 35 (2002) 782–790.
[43] C.P. Horwitz, D.R. Fooksman, L.D. Vuocolo, S.W. Gordon-wylie, N.J. Cox, T.J. Collins, Ligand design approach for securing robust oxidation catalysts, J. Am. Chem. Soc. 120 (1998) 4867–4868.
[44] T.J. Colins, C.P. Horwitz, A.D. Ryabov, L.D. Vuocolo, S. Sen Gupta, A. Ghosh, N.L. Fattaleh, Y. Hangun, B. steinhoff, C.A. Noser, E. Beach, D. Prasuhn Jr., T. Stuthridge, K.G. Wingate, J. Hall, L.J. Wright, I. Suckling, R.W. Allison, Tetraamido macrocyclic ligand catalytic oxidant activators in the pulp and paper industry, ACS Symp. Ser. 823 (2002) 47–60.
[45] S. Sen Gupta, M. Stadler, C.A. Noser, A. Ghosh, B. Steinhoff, D. Lenoir, C.P. Horwitz, K.W. Schramm, T.J. Collins, Rapid total destruction of chlorophenols by activated hydrogen peroxide, Science 296 (2002) 326–328.
[46] Y. Hangun, L. Alexandrova, S. Khetan, C.P. Horwitz, A. Cugini, D.D. Link, B. Howard, T.J. Collins, Oxidative desulfurization of fuels through TAML® activators and hydrogen peroxide: sulfur removal from gasoline and distillate streams, Prepr.-Am. Chem. Soc., Div. Pet. Chem. 47 (2002) 42–44.
[47] D.-L. Popescu, A. Chanda, M. Stadler, F. Tiago de Oliveira, A.D. Ryabov, E. Münck, E.L. Bominaar, T.J. Collins, High-valent first-row transition-metal complexes of tetraamido (4N) and diamidodialkoxido or diamidophenolato (2N/2O) ligands: synthesis, structure, and magnetochemistry, Coord. Chem. Rev. 252 (2008) 2050–2071.
[48] S. Mondal, Y. Hangun-Balkir, L. Alexandrova, D. Link, B. Howard, P. Zandhuis, A. Cugini, C.P. Horwitz, T.J. Collins, Oxidation of sulfur components in diesel fuel using Fe-TAML® catalysts and hydrogen peroxide, Catal. Today 116 (2006) 554–561.
[49] R. Nakajima, I. Yamazaki, The mechanism of oxyperoxidase formation from ferryl peroxidase and hydrogen peroxide, J. Biol. Chem. 262 (1987) 2576–2581.
[50] M.B. Arnao, M. Acosta, J.A. Del-Rio, R. Varon, F. Garcia-Canovas, A kinetic study on the suicide inactivation of peroxidase by hydrogen peroxide, Biochim. Biophys. Acta 1041 (1990) 43–47.
[51] A. Ghosh, D.A. Mitchell, A. Chanda, A.D. Ryabov, D.L. Popescu, E.C. Upham, G.J. Collins, T.J. Collins, Catalase-peroxidase activity of iron(III)-TAML activators of hydrogen peroxide, J. Am. Chem. Soc. 130 (2008) 15116–15126.
[52] T.J. Collins, Essays on science and society: toward sustainable chemistry, Science 291 (2001) 48–49.
[53] D. Banerjee, A.L. Markley, T. Yano, A. Ghosh, P.B. Berget, E.G. Minkley Jr., S.K. Khetan, T.J. Collins, "Green" oxidation catalysis for rapid deactivation of bacterial spores, Angew. Chem. Int. Ed. 45 (2006) 3974–3977.
[54] A. Chanda, D.-L. Popescu, F. Tiago de Oliveira, E.L. Bominaar, A.D. Ryabov, E. Münck, T.J. Collins, High-valent iron complexes with tetraamido macrocyclic ligands: structures, Mössbauer spectroscopy, and DFT calculations, J. Inorg. Biochem. 10 (2006) 606–619.
[55] W.R. Gombotz, S.F. Wee, Protein release from alginate matrices, Adv. Drug Deliv. Rev. 31 (1998) 267–285.
[56] A. Hagen, G. Skjak-Braek, M. Dornish, Pharmacokinetics of sodium alginate in mice, Eur. J. Pharmaceut. Sci. 4 (Suppl. 1) (1996) 100.
[57] N. Nagasawa, H. Mitomo, F. Yoshii, T. Kume, Radiation-induced degradation of sodium alginate, Polym. Degrad. Stab. 69 (2000) 279–285.
[58] H.Y. Zhao, W. Zheng, Z.X. Meng, H.M. Zhou, X.X. Xu, Z. Li, Y.F. Zheng, Bioelectrochemistry of hemoglobin immobilized on a sodium alginate-multi wall carbon nanotubes composite film, Biosens. Bioelectron. 24 (2009) 2352–2357.
[59] Patents of the Collins group including the key experimental procedures at http://www.chem.cmu.edu/groups/Collins/awardpatpub/patents/index.html.
[60] J.L. Wu, Y. Feng, T.L. Zhang, S.Y. Liu, L.Z. Meng, Y.B. He, Improvement to the syntheses of benzo-tetraamidemacrocyclic ligand, J. Wuhan Univ. (Nat. Sci. Ed.) 48 (2002) 442–444.
[61] A. Ghosh, F.T. Oliveira, T. Yano, T. Nishioka, E.S. Beach, I. Kinoshita, E. Münck, A.D. Ryabov, C.P. Horwitz, T.J. Collins, Catalytically active μ-oxodiiron(IV) oxidants from iron(III) and dioxygen, J. Am. Chem. Soc. 127 (2005) 2505–2513.
[62] R.W. Murray, Chemically modified electrodes, in: A.J. Bard (Ed.), Electroanalytical Chemistry, Marcel Dekker, New York, 1984, pp. 191–368.